



Automatic system for deformation measurement of anodes in an electrolytic process

F.J. delaCalle^{a,*}, A. Fernández^b, D.G. Lema^a, R. Usamentiaga^a, D.F. García^a

^a Universidad de Oviedo, Campus de Gijón, Gijón, 33204, Asturias, Spain

^b Iturcemi S.L., Avenida de la Siderurgia, Avilés, 33490, Asturias, Spain

ARTICLE INFO

Keywords:

Industrial automation
Computer vision
Industrial control
Electrolysis
Industrial inspection
Image processing

ABSTRACT

This paper proposes a novel system for measuring the deformation of anodes automatically in an electrolytic process, eliminating the need for manual intervention. The system employs cameras to acquire lateral perspective images of the anodes. These images are processed using a computer vision algorithm to give measurements of anode deformation, while considering potential errors arising from scene and object geometry. The system's results align with measurements conducted by operators across 71 anodes and were validated over 3900 more anodes in four different locations under different lightning and environmental conditions. This system improves efficiency, by automating a task that was previously carried out manually, and also safety by eliminating the operators need of handling heavy loads and operating in hazardous environments.

1. Introduction

Current industries are evolving into a new type of environment in which many tasks, previously manual, are now automatic [1]. This evolution is leading to faster and more efficient processes [2]. However, some critical tasks are still being performed by human operators, who are prone to mistakes due to fatigue. One of these tasks is the supervision of the deformation of the anodes in electrolytic facilities. The aim of this paper is to propose a new system that automates the measuring of the deformation in anodes in a electrolytic process. This task is usually performed by operators using manual tools.

Electrolysis is a method employed to decompose compound elements using electrical energy. This process, crucial for producing materials like aluminum, sodium, magnesium or zinc relies on two essential components working as electrodes: anodes and cathodes.

During the electrolytic process the anodes are bended in such a way that their shape becomes similar to a roof tile. After the anodes are extracted from the electrolytic cell, they are transported to a maintenance location where they are straighten before being reused. Although the anodes are straightened before being reused, they bend more each time they are used.

The efficiency of the process relies on the correct position of the anodes and cathodes in the electrolytic cells. They must be separated at a correct distance in order that the metal ions of metal in the solution are reduced at the surface of the cathodes, forming a layer of pure

metal. The deformation of the anodes results in non-uniform distances between the anodes and cathodes.

Deformed anodes must be straightened and checked before each set of anodes is carried back to an electrolytic cell. If an anode with a huge deformation is transported to a cell, it can collide with the cathodes already in the cell. This should be completely avoided due to the economic and material losses it can produce.

This paper proposes a computer vision system to measure the deformation in anodes. This system allows the human operator to check the deformation in anodes and reject some of them for reuse to prevent collisions and efficiency losses. Furthermore, as the measurement of the deformation of the anodes is still a manual and cumbersome process, the proposed system provides a way of save time and money inspecting the anodes automatically.

Computer vision is now broadly used in many fields such as pharmaceutical, automotive, aerospace and semiconductors [3]. Specifically in the metal industry, computer vision techniques have become essential to carry out many tasks such as quality control [4,5] or automatic guidance [6]. These new applications have improved the efficiency of the industrial facilities in many stages of product manufacturing [7] as they can automatically perform tasks that otherwise would be done manually by inspectors, sometimes in dangerous environments. Furthermore, they are used to improve the safety of the personnel as they can be used to detect people in dangerous environments or even detects the PPEs (Personal Protective Equipment) [8,9].

* Corresponding author.

E-mail addresses: delacalle@uniovi.es (F.J. delaCalle), adrian.fernandez@iturcemi.com (A. Fernández), gonzalezdario@uniovi.es (D.G. Lema), rusamentiaga@uniovi.es (R. Usamentiaga), dfgarcia@uniovi.es (D.F. García).

<https://doi.org/10.1016/j.measurement.2024.115626>

Received 5 June 2024; Received in revised form 27 August 2024; Accepted 28 August 2024

Available online 31 August 2024

0263-2241/© 2024 The Author(s). Published by Elsevier Ltd. This is an open access article under the CC BY-NC license (<http://creativecommons.org/licenses/by-nc/4.0/>).

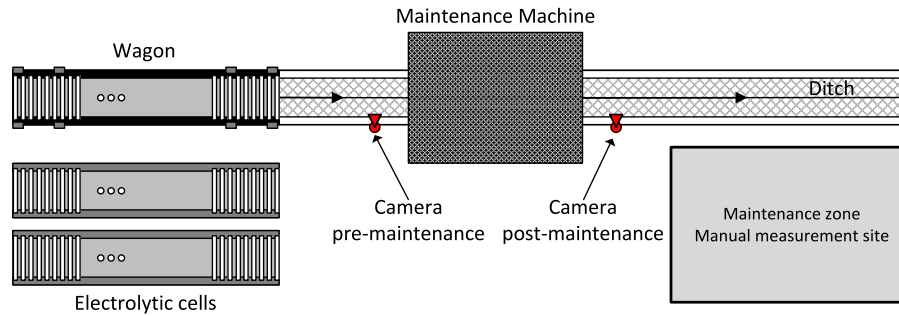


Fig. 1. Industrial context scheme.

Computer vision systems offer a distinct benefit in real-time monitoring and analysis of visual data in industrial settings. They can automatically identify specific situations and oversee the entire process in hazardous environments, all without putting human operators at risk. These systems also offers an great improvement in efficiency as they can detect defects in real-time [10].

Measuring the deformation of the anodes in an electrolytic facility using an automatic system provides a big improvement in efficiency and also prevents the operators from manipulating these heavy loads that can end up producing accidents. In fact, this kind of system reduces the need of the operator to be near the electrodes, which can be a hazardous environment [11].

Although computer vision techniques are widely used in the industry, there are other methods for monitoring industrial components that use different types of sensors. For example, vibration sensors can be employed to monitor machines involved in various parts of a production process [12] or to predict the lifespan of motors and other types of machinery [13].

The electrolytic process in which the proposed system is developed has a maintenance zone for the anodes in which their deformations are corrected right after each iteration of the electrolytic process, while the metal is extracted from the cathodes. The anodes of one electrolytic cell are lifted by a crane and deposited in a wagon that moves them to the machine that corrects the deformations. The aim of the electrolytic facility is to measure the deformation of the anodes during this process, before and after the correction. This scenario is shown in Fig. 1.

The wagon with the anodes goes through a pair of rails placed on the floor, so the anodes are located in a ditch. The manual system used now to measure the deformation of the anodes consists of lifting each anode from the wagon using a crane, measure the distance between the plane that connects the edges of the anode and the deepest point in the center of it. To do so, the operators use a specialized tool. This tool is a bar with four protrusions in the middle going from 1 cm to 4 cm in height. They put the tool touching both edges of the anode and check which one of the protrusions is the one that fits better the gap in the center of the anode. Thus, the operators obtain rough measurement of the deformation. For example, if the protrusion of 2 cm does not fit in the gap but the 1 cm one does, then, the deformation is measured as a 1 cm deformation, which means that the deformation goes from 1 cm to 2 cm. In Fig. 2 the deformation, D , of the anodes is defined schematically as well as the tool used to measure it. To facilitate understanding of the context, Fig. 3 provides a diagram showing a non-deformed anode and a deformed one. Along with these diagrams, several real examples of anodes are shown, along with the deformation measured manually by the operators. The manual process is inaccurate, cumbersome and requires so much time, so it is performed periodically but not after each iteration of the electrolytic process.

The facility has already developed a system capable of checking the correct state of the cathodes in the electrolytic process [14]. This paper shows the implementation of the supervision system in the part of the process concerning the anodes.

2. Materials and methods

2.1. Measurement concept

In this section, the proposed system will be described. The system must include sensors to measure the deformation of the anodes. The only place to locate any sensor for the new system is inside the ditch before and after the machine that corrects the deformation. The available space and the features of the ditch, and the anodes wagon, restrict the options for implementing the new system. Two technologies are the most commonly used to detect defects and measure features in metal industry: traditional images [15] and 3D vision [4]. 3D vision techniques, mostly represented by photogrammetry and laser reconstruction, need certain angles to measure the deformation correctly. Due to the proximity of the anodes in the wagon (270 mm), the field of view of 3D sensors is not suitable for developing the system. Therefore, traditional imaging will be utilized instead.

The cameras that will acquire images of the anodes to measure the deformation will be placed on the sides of the ditch. These cameras will acquire images of the anodes from their side. Some anodes suffer a second type of deformation that twist them a bit. Therefore, the measure obtained will not be exactly the deformation of the anode. In Fig. 4, the options of the projections of the anode in the image, taken from one side, are shown. In this image four scenarios are shown depending on the deformations of the anode. In these scenarios, the measurement taken by the system, M , is compared with the real measure of the deformation, D .

Defining the anode as an arc, the difference between de deformation, D , and the measurement taken by the system, M , can be defined using the center of the arc, C , and two points, L and R , defined as follows. The measurement is a segment defined by a Left point, L , and a Right point, R , and the projection of the arc, the anode, in the horizontal axis. L and R are defined in (1) and (2) respectively where C is the center of the arc a .

$$l = (C_x - a_{radius}, C_y); L = \begin{cases} l & l \parallel a \\ a_{left} & l \nparallel a \end{cases} \quad (1)$$

$$r = (C_x + a_{radius}, C_y); R = \begin{cases} r & r \parallel a \\ a_{right} & r \nparallel a \end{cases} \quad (2)$$

Thus, the difference of between the measurement made by the system and the real deformation can be seen in Fig. 5 in which the length of the arc remains constant as it is a solid metal plate and the variations are made in the rotation of the arc and the angle of the arc itself. As shown in the figure, the error increases with the rotation and the angle. However, the facility in which the system is installed prevents the rotation by adding a rigid frame at the top of them, which is also used to move them, so the rotation is minimized and can be assumed as 0.5° in the worst scenario, which implies an error that depends on the deformation of the anode as shown in Table 1.

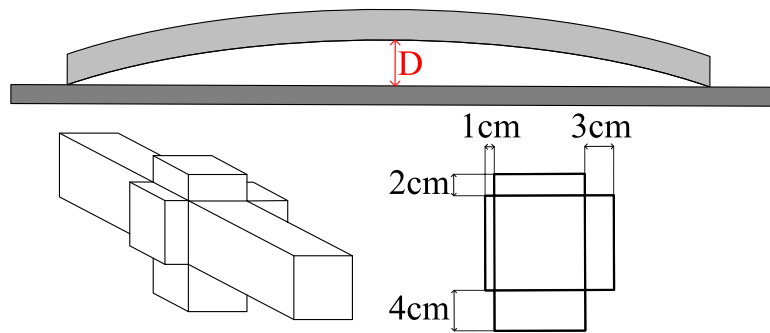
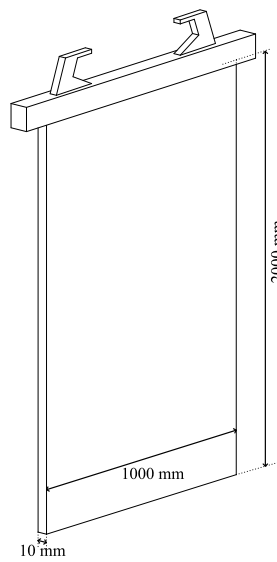
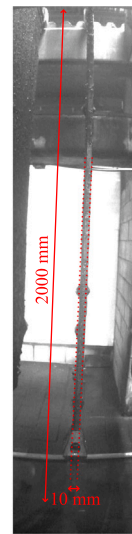


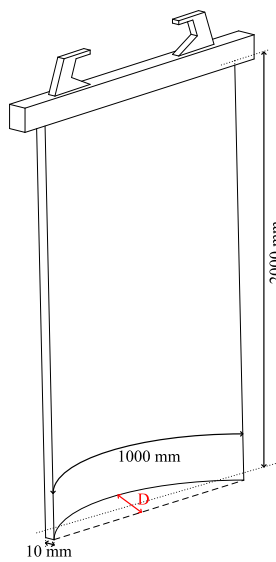
Fig. 2. Deformation of the anode and measuring tool.



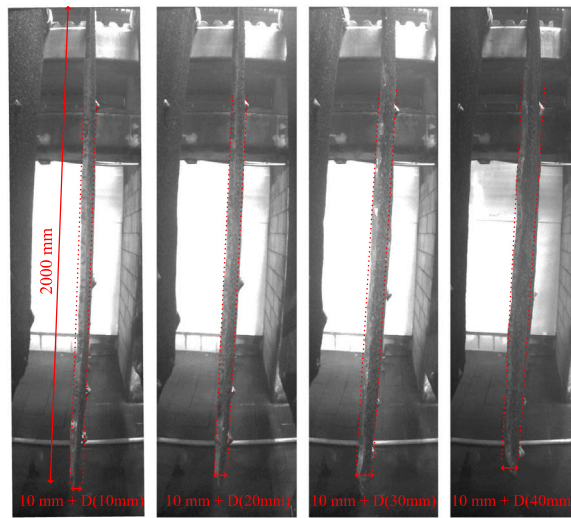
(a) Non-deformed anode scheme



(b) Non-deformed anode example



(c) Deformed anode scheme



(d) Deformed anodes examples

Fig. 3. Deformed and non-deformed anodes examples.

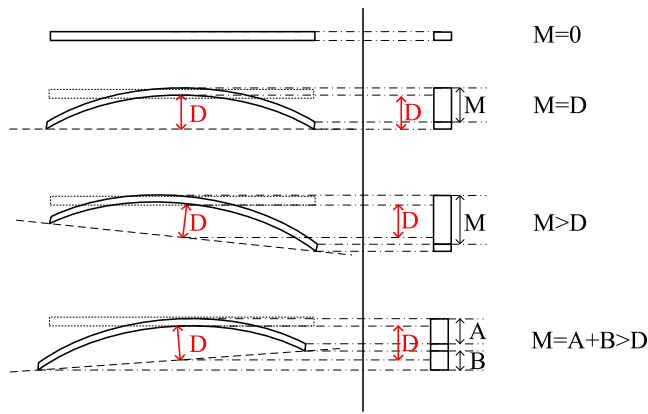


Fig. 4. Measure of the deformation from the side.

Table 1
Error of the system by anode deformation for 0.5° rotation.

Deformation	Error
From 0 mm to 10 mm	5.31 mm
From 10 mm to 20 mm	4.67 mm
From 20 mm to 30 mm	4.54 mm
From 30 mm to 40 mm	4.48 mm
More than 40 mm	4.44 mm

2.2. Proposed method

The proposed computer vision method is divided in three stages. These stages are briefly described below and shown in Fig. 6. They will also be described in detail in the next sections, that are also labeled as they appear in Fig. 6.

First, the image of the anode must be acquired and rectified in order to eliminate distortions produced by camera lens and establish a relation between pixel magnitudes and real-world magnitudes. These operations are described in the Image Acquisition section.

Once the rectification is performed, the image goes through a local adaptive threshold to extract the edges present in the image. This operation is configured in such a way that it focuses on objects similar to the size they anode should have. Then, from all the edges detected, the ones from the anode are located. At this point, the edges of the anode include some material that is still adhered to the surface of the anode. In order to eliminate that material an opening operation is performed. These operations are described in the Image Processing section.

Finally, the deformation of the anode must be measured. As the segmentation can present errors due to the presence of other objects in the image, even in the background, several measuring areas are set for redundancy. The intersection between these areas and the detected edges is performed and then measured to give a magnitude of the deformation of the anode. These operations are described in the Measuring the Deformation section.

2.2.1. Image acquisition

The industrial context implies that the cameras of the system will be placed in a ditch. Therefore, the illumination conditions will be poor but at the same time will vary from one ditch to another because of the environmental light of the factory. Thus, the type of camera used in the system should be able to adapt its parameters so that it can acquire an image maintaining the main features of the image constant. The selected camera is a MOBOTIX Mx-M73A-RJ45 that can also acquire images with a dynamic exposure time that meets the challenges of these illumination conditions always providing similar images. This camera is designed for video-surveillance, which makes it cheaper than computer vision cameras, reducing the cost of the system significantly.

The camera adapts its parameters dynamically so that the images acquired maintains similar luminance. This makes the processing software much simpler and portable to other facilities.

The initial step in the image processing methodology involves rectifying the image and mapping it to real-world coordinates. This rectification process necessitates accurate calibration of the camera [16]. Image rectification yields an image wherein objects can be readily measured.

Calibrating a pinhole camera entails determining both its intrinsic and extrinsic parameters to mitigate any distortions in the acquired images. Intrinsic parameters pertain to internal characteristics like focal length, principal point, and image sensor size, while extrinsic parameters denote the camera's position and orientation relative to the 3D world.

The calibration process aims to estimate the intrinsic and extrinsic parameters using a series of images of a calibration target with known 3D coordinates. The relationship between the 3D coordinates of the calibration target, X , and the 2D image coordinates, x , is articulated in (3), where s represents a scaling factor, K signifies the camera intrinsic matrix, R denotes the rotation matrix depicting the camera's orientation, t stands for the translation vector delineating the camera's position, and $[R|t]$ constitutes the extrinsic matrix amalgamating the rotation and translation parameters.

$$s \cdot x = K \cdot [R|t] \cdot X \quad (3)$$

The intrinsic matrix, K , is defined in (4), where f_x and f_y are the focal lengths in the x and y directions and c_x and c_y are the coordinates of the center point.

$$K = \begin{bmatrix} f_x & 0 & c_x \\ 0 & f_y & c_y \\ 0 & 0 & 1 \end{bmatrix} \quad (4)$$

To estimate the camera parameters, the intrinsic and extrinsic matrices that minimize the error between the observed image coordinates, x , and the predicted coordinates obtained using the 3D coordinates, X , and camera matrices must be calculated. This can be done using a nonlinear optimization such as Levenberg–Marquardt.

Lens distortion can introduce significant errors in acquired images. To mitigate this distortion, a radial distortion correction model is used. The radial distortion model assumes that distortion can be approximated using a radial polynomial function. Distortion correction is applied to pixel coordinates of the acquired image. Mathematically, radial distortion correction can be expressed as (5) where x_c is the corrected pixel coordinate, x is the original pixel coordinate, r is the radial distance from the principal point and k_1, k_2, k_3, \dots are the radial distortion coefficients.

$$x_c = x (k_1 r^2 + k_2 r^4 + k_3 r^6 + \dots) \quad (5)$$

Once the camera is calibrated, the estimated parameters can be used to rectify the image. The rectification process involves calculating a set of homography matrices that map the distorted image coordinates to the rectified image coordinates. The homography matrix, H , can be calculated as (6), where R_1 and R_2 are the rotation matrices that align the epipolar lines of the rectified image, and t_1 and t_2 are the translation vectors that move the camera to the rectified position.

$$H = K \cdot [R_1|t_1] \cdot R \cdot [R_2|t_2]^{-1} \cdot K^{-1} \quad (6)$$

The rectification homography can be applied to the original image using image warping, which involves mapping each pixel (u, v) in the original image to its corresponding pixel (u', v') in the rectified image using the homography matrix H (7).

$$[u', v', 1] = H \cdot [u, v, 1] \quad (7)$$

Once the pixels are mapped, the pixel values from the original image are interpolated into the rectified image to obtain the final rectified image. The result of this step is shown in Fig. 7. Then the image is cropped

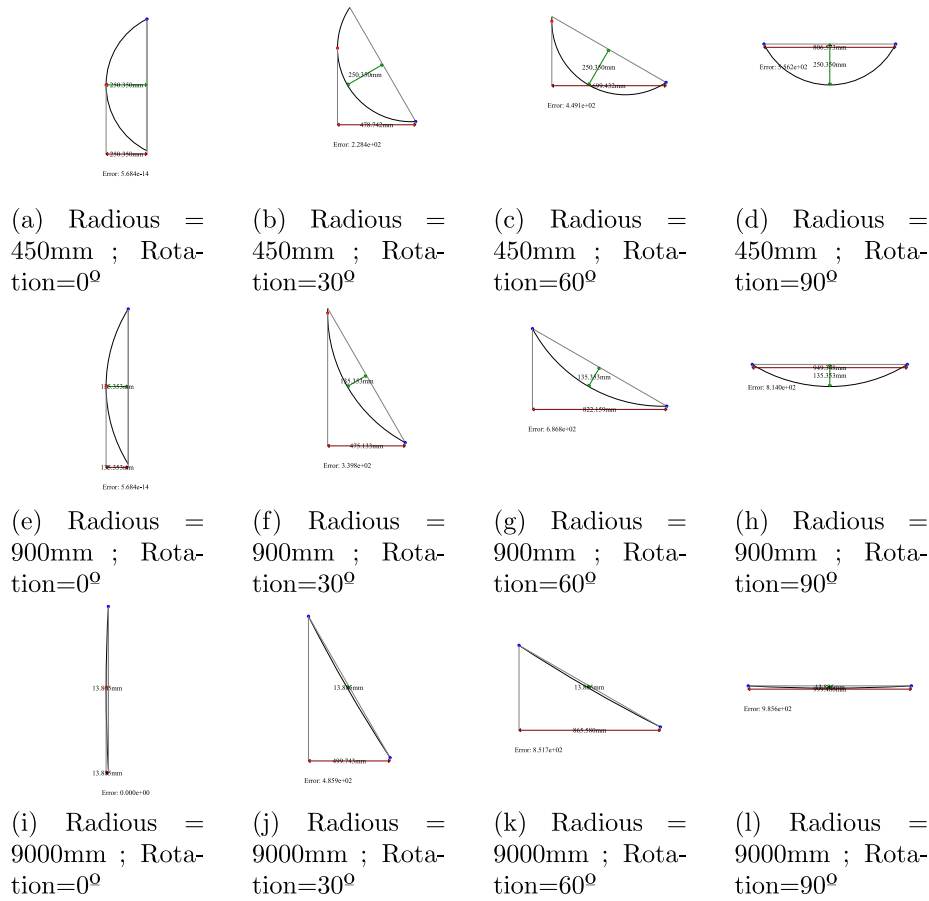


Fig. 5. Differences between the real deformation and the measurement made by the system.

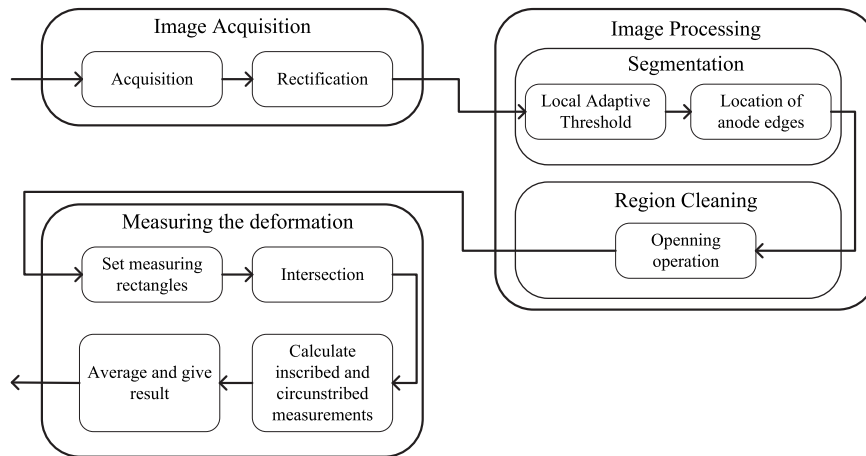


Fig. 6. Proposed method scheme.

in order to have a rectangular image as the corners of the rectified image will never give relevant information so they can be discarded. The image processing algorithm will then work with rectangular images in which magnitudes in pixels can be easily translated into real world magnitudes.

The measurement procedure, described in Section 2.1 analytically, on the correct placement of the anodes in front of the camera to avoid measurement errors caused by non-orthogonal acquisitions. The best way to ensure that the anodes are in the correct position during acquisition is mechanically. A stop system controlled by a photocell has been installed in the wagon that carries the anodes. When the

photocell detects an anode in the acquisition position, it stops the wagon, captures the image, and then continues the movement. Since the total time required for the electrolysis process far exceeds the time needed for anode maintenance, stopping the wagon to capture images does not cause any delays in the production line.

2.2.2. Image processing

The first step is the segmentation of the anode. To do so a local threshold is performed. As the location of the camera is known and the anode is expected to be in the middle of the image, a ROI can be set statically for each deployment of the system in order to process

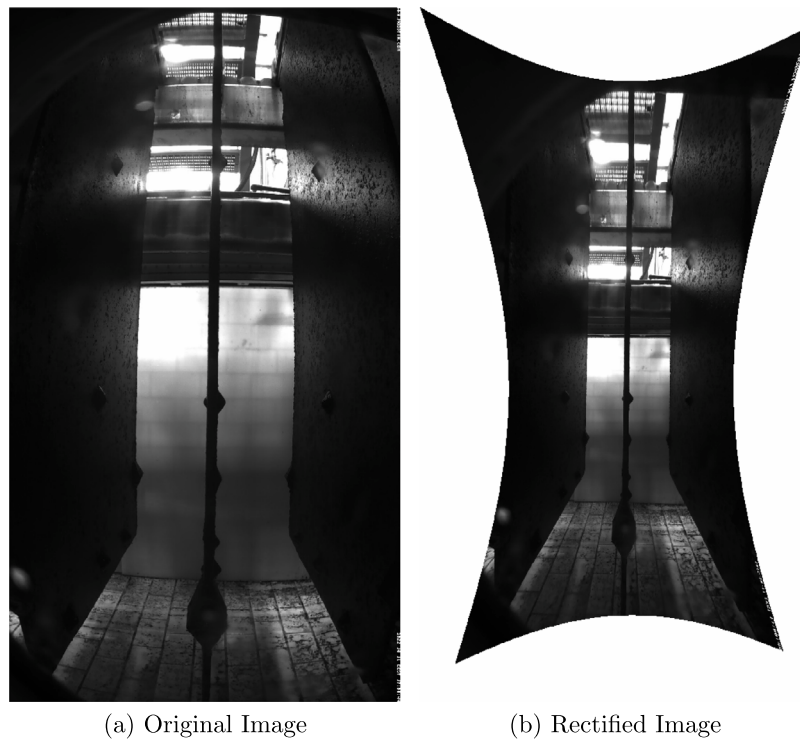


Fig. 7. Rectification of an image.

just a region of the image, speeding up the whole process. In Fig. 8 two images are used to illustrate the entire process. One of them corresponds to an image of an anode before the maintenance process (Fig. 8(a)), implying that it still has a lot of material adhered to it and is in very unfavorable lighting and dirt conditions. The other image (Fig. 8(e)) corresponds to an anode after the maintenance process, cleaner and in an area with less dirt and more favorable lighting conditions. In this way, a favorable case and an unfavorable one are exemplified. To demonstrate the process on an anode with a severe deformation, Fig. 9 has also been included, showing the process on an anode with a deformation of 4 cm.

The segmentation process selects from the image those regions in which the pixels fulfill a threshold condition. Let g_o be the pixel value of the original image and g_t be the pixel value of the threshold image, then the condition of selection can be expressed as (8) where *Offset* is a control parameter to control the size of the regions extracted. The larger offset is chosen the smaller the extracted regions. The threshold image should be a smoothed version of the original image obtained by applying a lowpass filter, a mean filter is chosen in this case. Thus, the effect of the process is similar to applying a thresholding operation to a highpass-filtered version of the original image. In addition, as the image itself is used after a lowpass filter to be compared with the original image, the thresholding operation can adapt to different lighting conditions.

$$g_0 \leq g_t + Offset \quad (8)$$

This segmentation process extracts the contours of an object, where the size of the object is determined by the mask size of the lowpass filter. The larger the mask size is chosen, the larger the found regions become. As a rule of thumb, the mask size should be about twice the diameter of the objects to be extracted. In this case, as the image is rectified and the pixels represent millimeters in the image, the size of the mask can be calculated physically using the size of the anode and the size of its maximum deformation, that is $10 + 40 = 50$ mm.

As there is no other method that can extract and measure the anode to be used as comparison, the best way to compare the efficiency of

the system is the segmentation step. Thus, the method is also set to use other segmentation method to extract the edges of the anode. The results of this options will be given in Section 3 including Canny [17], Deriche [18], Lanser [19] and Shen–Castan [20] methods.

Once all the detected edges are extracted from the image, the edges corresponding to the anode need to be identified. To accomplish this, a measurement rectangle is placed vertically in the middle of the image, covering most of the region of interest (ROI) where the measurement should be taken. The intersection between this rectangle and the detected edges is then calculated.

Next, an opening operation is performed on the intersected regions to eliminate background noise. This operation uses a rectangular mask, with its width set to a quarter of the measurement rectangle's width and its height set to half of the expected anode size. The center of gravity of the resulting region is then used to define a local ROI where the measurement will be conducted.

This new ROI is generated based on the anode's physical dimensions as follows: 10 mm for the anode size, 40 mm for the maximum deformation, plus an additional 10 mm for securing reasons.

In Figs. 8(b) and 8(f) this first step is shown. The extracted edges are shown in red, the measurement rectangle in green and the new ROI in blue.

The region resulting from the intersection between the ROI and the edges must be refined to remove any material adhered to the anode that might affect the measurement. Additionally, as shown in the images, the anodes have a series of rubber separators that also need to be removed for accurate measurement. This refinement is accomplished using an opening operation with a rectangular mask. Since the largest objects to be removed are the rubber separators, the mask size should match their size. Therefore, the mask is set to 1 pixel in height and the width of the rubber separators (80 mm, converted into pixel units). The results of this cleaning operation are shown in Figs. 8(c) and 8(g), where the ROI is shown in blue and the extracted region representing the anode is shown in red.

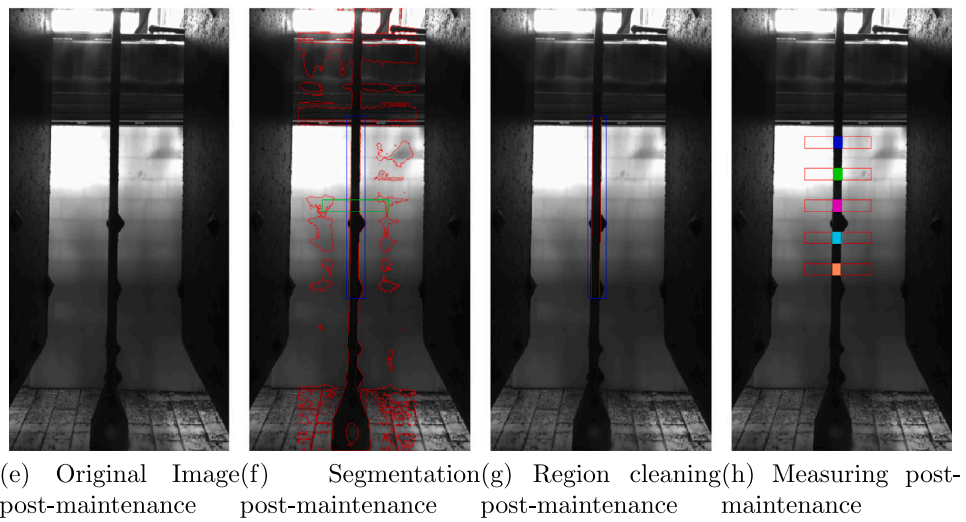
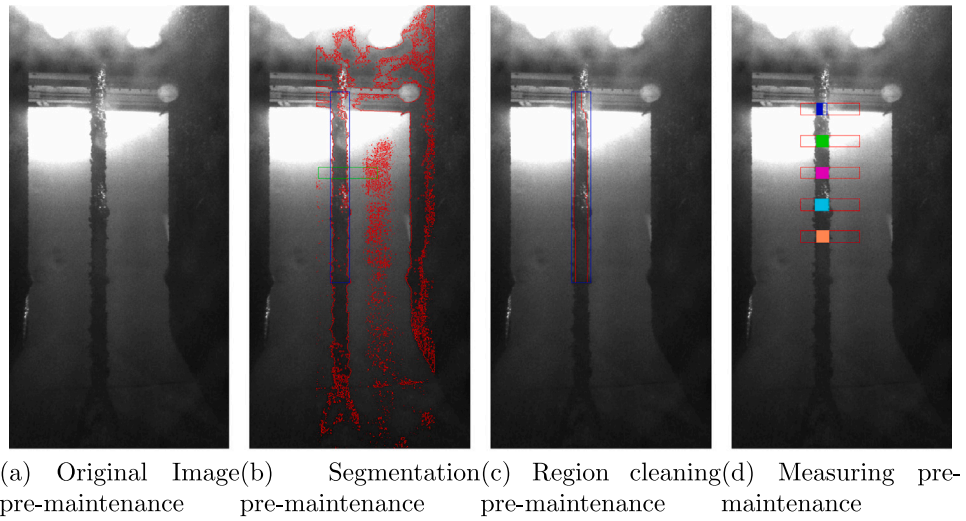


Fig. 8. Image processing procedure.

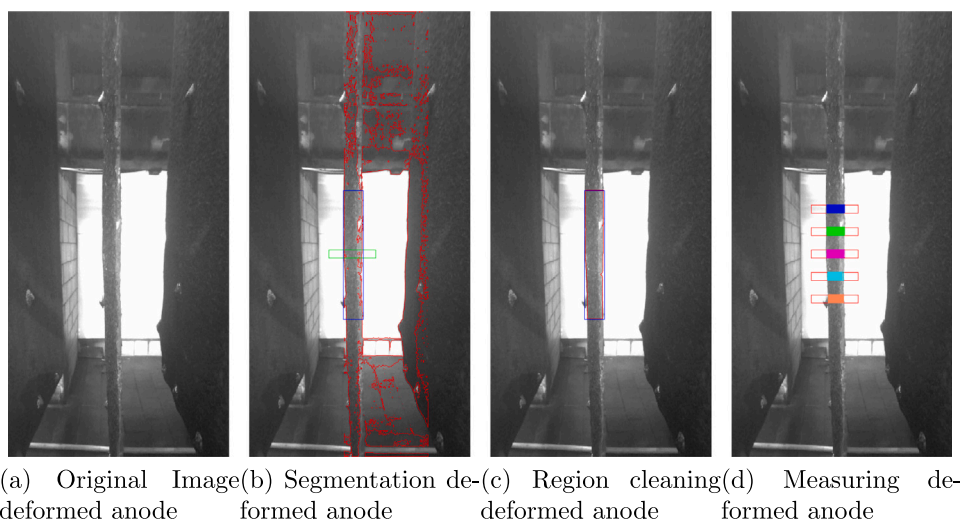


Fig. 9. Image processing procedure of a deformed anode.

2.2.3. Measuring the deformation

Once the anode shape is extracted as seen in previous sections, it must be measured in order to estimate the deformation. Extracting just one measure of the anode could lead to errors and uncertainty, so the anode is measured in several positions. As seen in Figs. 8(d) and 8(h) five measuring rectangles are set. The intersection between these rectangles and the extracted shape is calculated, producing five different regions in the image.

The extracted regions are then used to measure the deformation. As these regions shall not be regular, the measurement they represent can be done using two different approaches. The first approach assumes that any area within these regions that deviates from a regular shape represents material adhered to the anode or noise. Therefore, the best possible measure would be the calculation of the rectangle inscribed within the region. The second approach considers that segmentation may fail in some areas, resulting in a non-regular region due to glare, reflections, or lens dirt issues. Under this second viewpoint, the most accurate calculation would be obtained by calculating the rectangle circumscribed around the region. Both approaches are valid and reasonable, so the most conservative option is to take an average of both measurements. As can be seen in Figs. 8(d) and 8(h), discrepancies between the measurements of the inscribed and circumscribed rectangles are not very common, exemplified only in the leftmost measurement in Fig. 8(d) as a problematic case.

The measure obtained in pixels, could be directly translate to real world units, but it will not give an accurate measure of the deformation D . In this measurement, the thickness of the anode is still present and should be eliminated. Moving the pose of the camera is enough for calculating how many pixels should represent the 10 mm of thickness of the anode. Therefore, this number of pixels are subtracted from the previous measurement and the resulting amount is multiplied by the size of the pixel, giving a measurement of the deformation. However, as described in Section 2.1, the obtained magnitude is not the real magnitude D , it is M because of the rotation the anode can suffer (see Fig. 4). Therefore, the results given in next sections will take into account the error calculated in Table 1 in order to compare the measured magnitude of the deformation, M , with the real magnitude of the deformation, D .

Operators in the facility measure the deformation approximately in the area in which the middle rectangle is placed. The another 4 measurements are used to give a estimation of the reliability of the middle one. If each one of these measurements is similar to the middle one, a 25% of reliability is added to the middle one. The similarity is defined as being in the interval $middle \pm 5$ mm

3. Results and discussion

The proposed system must be tested under real lighting conditions with actual anodes. For this purpose, a series of images of anodes taken at an electrolysis plant are needed. During normal operation, the deformation of the anodes is not measured between all electrolysis cycles because the measurement procedure implies the facility to halt the production, making it costly to obtain measurements to compare the results of the system with the actual deformation of the anodes.

For the generation of a database of images labeled with the magnitude of the anode deformation, 71 anodes are extracted from the total number of anodes in the plant, ensuring they are distributed across different ranges of deformation magnitude. These anodes are manually measured by plant operators using the standard procedure showed in Fig. 2. This procedure provides a centimeter-scale deformation value called X , which means that the actual deformation belongs to the interval $[X, X + 1]$ cm. The Ground Truth provided by the electrolysis plant is presented in Table 2. Once measured, these anodes are transported to the wagon where the anodes that the system should measure are typically located. Then, the wagon is moved in front of the system's

Table 2

Ground truth provided by the electrolysis plant.

Magnitude of the deformation	Number of samples
From 0 mm to 10 mm	18
From 10 mm to 20 mm	13
From 20 mm to 30 mm	13
From 30 mm to 40 mm	13
More than 40 mm	14

camera to obtain images of the anodes from the ground truth database under the operating conditions of the final system.

The Ground Truth is then processed using the proposed system giving a measure of the deformation for each anode. These measurements must be given as an interval using the error calculated in Table 1. Therefore, each measurement is given as $Result \pm \frac{Error}{2}$. The results of processing the Ground Truth are shown in Fig. 10. These results show that only 5 of 71 anodes produce a result in which the interval of error is outside the limits of the Ground Truth. However, the mean value from each result is inside those limits given by the Ground Truth.

The results of processing the Ground Truth show that the system is capable of measuring the deformation of the anode matching the measurements made by the operators manually. As the operators must take the anodes out of the wagon in order to manually measure the deformation, this system speeds up the process significantly. The anodes are heavy loads that needs a crane in order to be lifted and manipulated, this manipulation made by an operator is dangerous and must be performed in a hazardous environment.

When anodes come out of the electrolysis cells, they have particles of manganese dioxide adhered to their surface. This substance is highly harmful, especially after prolonged exposure, as it can cause damage to the central nervous system [21]. These results show that the operators no longer need to perform this task manually, thus avoiding repeated and prolonged exposure to this harmful substance and thereby preventing intoxication due to it.

3.1. Validation

The system was tested in a facility with 71 anodes manually measured by operators. The generation of a Ground Truth with anodes perfectly measured by operators is an enormously costly task for the facility, as it implies that the facility's normal production must be halted while the anodes are transported, measured, and subsequently returned to their origin. To avoid this task, the system has been validated in a second recently commissioned electrolysis facility. Because of the facility has been recently commissioned, the anodes cannot have any deformation greater than 45 mm as this only occurs after continuous use in electrolysis cycles. Therefore, the system can be run over non-measured anodes and its results can be classified according to the fact that none of them should be greater than 45 mm.

The result provided by the system not only provides the measurement of deformation but also a reliability of the result derived from replicated measurements at various areas in the image, as explained in Section 2.2.3. Therefore, the results can be classified in 3 categories: Correct and reliable (less than 45 mm), Incorrect and reliable (more than 45 mm) and Not reliable.

To validate the system under the widest range of lighting and environmental conditions (such as suspended particles), four cameras are installed on four different maintenance lines, two before and two after the machine that corrects the deformation of the anodes. Therefore, the results will be given as L1 (Pre-Maintenance), L2 (Post-Maintenance), L3 (Pre-Maintenance) and L4 (Post-Maintenance). The differences between the conditions pre and post maintenance have already been shown in Fig. 8. In order to compare the results of the system with other methods, the system has been also configured to use Canny, Deriche, Lanser and Shen–Castan edge detectors in the segmentation step.

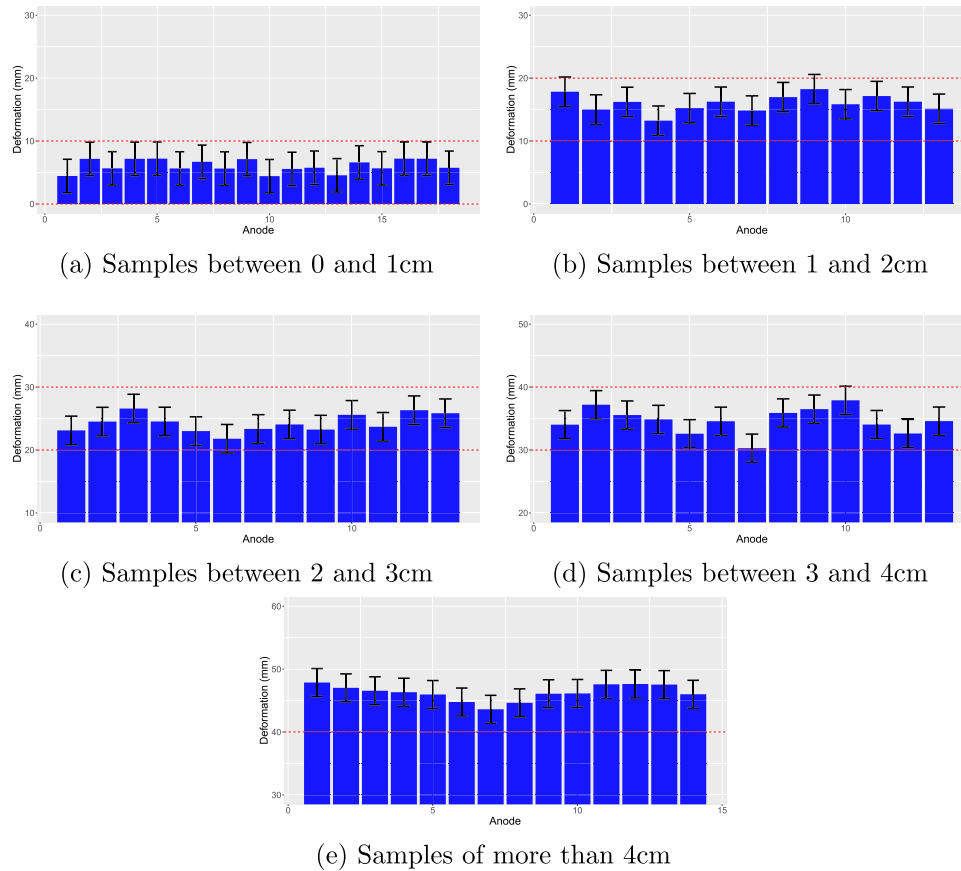


Fig. 10. Results of processing the Ground Truth.

After 6 days of operation, the results of the system for the 4 locations are shown in Table 3, giving the Recall as the number of Correct and reliable measurements divided by the number of samples. The results show that the anodes processed in the pre-maintenance zones, L1 and L3 are prone to give worse results in terms of reliability as they still have a lot of material adhered to them and the environmental conditions are worse. However, they still give a good result 87% and 89% of the times. These percentages are still far from the ones provided in post-maintenance zones, 96% and 95%. Therefore, the suggestion is to install the system after the maintenance machine. The deformation of the anodes is more important after maintenance as one of the objectives of the maintenance machine is to eliminate the deformation. Only the anodes that are still too deformed after maintenance should be rejected and replaced. However, it remains of interest to measure the deformation before the machine, as an excessively deformed anode could potentially block the machine, although this circumstance is highly unlikely.

The results provided by other segmentation methods are shown in Table 4 giving only the recall as a summary. Although all the methods give similar results in L2 and L4 zones, this is because these zones are post maintenance, with clear lightning conditions, no material adhered to the anodes and less dirty environment. The proposed method outperforms the others in the worst scenario zones, those from L2 and L4 as it can adapt better to the noise produced by the light and dirt and is specifically designed to detect an object of the anode characteristics. Therefore, the proposed method is more suitable to be installed in another facility with less configuration needed.

The system performs correctly with reliable results 91% of the times including zones pre and post maintenance. This will improve the traceability of the deformation of the anodes of the facility and will prevent errors and efficiency losses in the electrolysis process. As the operators do not need to lift the anodes for measuring manually the

Table 3

Results of the validation of the system.

	L1	L2	L3	L4	Total
Correct and reliable	431	296	2208	991	3926
Incorrect and reliable	0	0	13	0	13
Not reliable	59	11	251	44	365
Recall	0.879	0.964	0.898	0.957	0.915

Table 4

Recall comparison with other segmentation methods.

	L1	L2	L3	L4	Total
Proposed	0.879	0.964	0.898	0.957	0.915
Canny	0.827	0.941	0.854	0.951	0.881
Deriche	0.835	0.948	0.863	0.959	0.889
Lanser	0.831	0.938	0.861	0.956	0.886
Shen-Castan	0.851	0.962	0.886	0.961	0.905

deformation, the working conditions will be improved, preventing them from being in a hazardous environment which is also prone to accidents due heavy loads.

4. Conclusions

This paper proposes a novel method to measure the deformation of the anodes in an electrolytic facility dedicated to metal production. The proposed system uses a camera at each measurement point to capture the anodes from a lateral perspective. These images are processed, and a measurement of the anode deformation is obtained, considering the error that may be incurred due to the geometry of the scene and the object.

The task of measuring the deformation of the anodes is cumbersome since it is carried out manually by the facility operators. This task involves handling heavy loads in a hazardous environment due to substances like manganese dioxide. The proposed system eliminates the need to carry out this task manually, so it not only enhances process efficiency but also reduces the risk associated with manual handling of heavy loads and exposure to hazardous substances, thereby ensuring worker safety and preventing potential health hazards. Furthermore, the automatic measurement of the deformations, improves the efficiency of the facility and the traceability of the deformation of each anode between electrolytic cycles.

The manual inspection process cannot be carried out for each anode in every electrolysis cycle as it entails halting production, which incurs an unsustainable cost for the plant. The proposed system measures each anode, identified through RFID, after every electrolysis cycle, allowing the plant to track the deformation of each anode over time.

The system has been tested over 71 anodes that were measured in a real facility. The obtained results match the measurements made by the operators in the 71 anodes. In five of these anodes, the error interval given by the geometric conditions of the measurement exceeds the limits of manual measurement, even though the result obtained agrees with the manual measurement.

To validate the system, it was installed in 4 different locations in a real facility. The system was operating over 5 days in the four locations, processing more than 3900 anodes. The result of this validation gives correct results in 91.2% of the times validating the system in a real industrial environment.

Overall, the implementation of the proposed computer vision system offers a promising solution to the challenges faced in electrolytic processes, demonstrating significant improvements in efficiency, safety, and overall productivity within the industrial context. Below are the key findings from this work summarized:

- **Improved Accuracy:** The automated system enables precise measurement of each anode before and after maintenance avoiding manual measurements.
- **Increased Safety:** The need for manual interventions is significantly reduced and even eliminated, minimizing risks for operators.
- **Operational Efficiency:** The system's implementation does not interfere with the production time due to its rapid operation compared to the electrolysis process.
- **Successfully tested:** The system has been tested over 71 anodes giving the same results that the ones obtained by the facility operators with manual tools.
- **Broadly validated:** 91.2% of correct measurements over more than 3900 anodes.
- **Adaptive operation:** Validation was carried out in 4 different locations proving that the proposed method can adapt itself to different conditions giving similar results.

CRedit authorship contribution statement

F.J. delaCalle: Writing – review & editing, Writing – original draft, Validation, Software, Investigation, Formal analysis. **A. Fernández:** Visualization, Software, Resources, Investigation. **D.G. Lema:** Visualization, Software, Investigation. **R. Usamentiaga:** Supervision, Project administration, Conceptualization. **D.F. García:** Supervision, Project administration, Conceptualization.

Declaration of competing interest

The authors declare that they have no known competing financial interests or personal relationships that could have appeared to influence the work reported in this paper.

Data availability

The authors do not have permission to share data.

Acknowledgments

The authors would like to thank engineers and personnel of Delta Digital, Iturcemi group, for their help in the development of this research. This work has been partially funded by the project MCIU-22-PID2021-124383OB-I00 of the Spanish State Plan for Scientific and Technical Research and Innovation 2021–2023 and by the project FUIO-21-195 by Iturcemi S.L.

References

- [1] E. Oztemel, S. Gursev, Literature review of industry 4.0 and related technologies, *J. Intell. Manuf.* 31 (2020) 127–182, <http://dx.doi.org/10.1007/s10845-018-1433-8>.
- [2] V. Azamfirei, F. Psarommatis, Y. Lagrosen, Application of automation for in-line quality inspection, a zero-defect manufacturing approach, *J. Manuf. Syst.* 67 (2023) 1–22, <http://dx.doi.org/10.1016/j.jmsy.2022.12.010>.
- [3] Z. Liu, H. Ukida, K. Niel, P. Ramuhalli, *Industrial Inspection with Open Eyes: Advance with Machine Vision Technology*, Springer London, London, 2015, pp. 1–37, http://dx.doi.org/10.1007/978-1-4471-6741-9_1.
- [4] F.J. delaCalle, D.F. García, R. Usamentiaga, Rail surface inspection system using differential topographic images, *IEEE Trans. Ind. Appl.* 57 (3) (2021) 2994–3003, <http://dx.doi.org/10.1109/TIA.2021.3059605>.
- [5] R. Usamentiaga, D.F. García, F.J. delaCalle, Automated virtual gauges for dimensional quality control, *IEEE Trans. Ind. Appl.* 57 (3) (2021) 2983–2993, <http://dx.doi.org/10.1109/TIA.2021.3057353>.
- [6] E. Vrochidou, D. Oustadakis, A. Kefalas, G.A. Papakostas, Computer vision in self-steering tractors, *Machines* 10 (2) (2022) <http://dx.doi.org/10.3390/machines10020129>.
- [7] L. Zhou, L. Zhang, N. Konz, Computer vision techniques in manufacturing, *IEEE Trans. Syst. Man Cybern.* 53 (1) (2023) 105–117, <http://dx.doi.org/10.1109/TSMC.2022.3166397>.
- [8] D.G. Lema, R. Usamentiaga, D.F. García, Low-cost system for real-time verification of personal protective equipment in industrial facilities using edge computing devices, *J. Real-Time Image Process.* 20 (6) (2023) 1–18, <http://dx.doi.org/10.1007/s11554-023-01368-7>.
- [9] A.S. Kulinan, M. Park, P.P.W. Aung, G. Cha, S. Park, Advancing construction site workforce safety monitoring through bim and computer vision integration, *Autom. Constr.* 158 (2024) 105227, <http://dx.doi.org/10.1016/j.autcon.2023.105227>.
- [10] A. Ettalibi, A. Elouadi, A. Mansour, Ai and computer vision-based real-time quality control: A review of industrial applications, *Procedia Comput. Sci.* 231 (2024) 212–220, <http://dx.doi.org/10.1016/j.procs.2023.12.195>, 14th International Conference on Emerging Ubiquitous Systems and Pervasive Networks / 13th International Conference on Current and Future Trends of Information and Communication Technologies in Healthcare (EUSPN/ICTH 2023).
- [11] Z. Ma, L. Duan, J. Jiang, J. Deng, F. Xu, L. Jiang, J. Li, G. Wang, X. Huang, W. Ye, Y. Wen, G. Zhang, N. Duan, Characteristics and threats of particulate matter from zinc electrolysis manufacturing facilities, *J. Clean. Prod.* 259 (2020) 120874, <http://dx.doi.org/10.1016/j.jclepro.2020.120874>.
- [12] I. Aldekoa, A. del Olmo, L. Sastoque-Pinilla, S. Sendino-Mouliet, U. Lopez-Novoa, L.N.L. de Lacalle, Early detection of tool wear in electromechanical broaching machines by monitoring main stroke servomotors, *Mech. Syst. Signal Process.* 204 (2023) 110773, <http://dx.doi.org/10.1016/j.ymssp.2023.110773>.
- [13] L. Magadán, J. Granda, F. Suárez, Robust prediction of remaining useful lifetime of bearings using deep learning, *Eng. Appl. Artif. Intell.* 130 (2024) 107690, <http://dx.doi.org/10.1016/j.engappai.2023.107690>.
- [14] F.J.d.l. delaCalle, A. Gómez, D.F. García, R. Usamentiaga, Location monitoring system to prevent falls of cathodes in industrial electrolysis facilities, *IEEE Trans. Ind. Appl.* (2024) 1–11, <http://dx.doi.org/10.1109/TIA.2024.3384142>.
- [15] F. López de la Rosa, J.L. Gómez-Sirvent, R. Morales, R. Sánchez-Reolid, A. Fernández-Caballero, Defect detection and classification on semiconductor wafers using two-stage geometric transformation-based data augmentation and squeeze-net lightweight convolutional neural network, *Comput. Ind. Eng.* 183 (2023) 109549, <http://dx.doi.org/10.1016/j.cie.2023.109549>.
- [16] Y.-J. Zhang, Camera calibration, 2023, pp. 37–65, http://dx.doi.org/10.1007/978-981-19-7580-6_2.

- [17] J. Canny, A computational approach to edge detection, *IEEE Trans. Pattern Anal. Mach. Intell.* PAMI-8 (6) (1986) 679–698, <http://dx.doi.org/10.1109/TPAMI.1986.4767851>.
- [18] R. Deriche, Using canny's criteria to derive a recursively implemented optimal edge detector, *Int. J. Comput. Vis.* 1 (1987) 167–187.
- [19] S. Lanser, W. Eckstein, A modification of deriche's approach to edge detection, 3 (1992) 633–637. <http://dx.doi.org/10.1109/ICPR.1992.202067>.
- [20] J. Shen, S. Castan, An optimal linear operator for step edge detection, *CVGIP, Graph. Models Image Process.* 54 (2) (1992) 112–133, [http://dx.doi.org/10.1016/1049-9652\(92\)90060](http://dx.doi.org/10.1016/1049-9652(92)90060).
- [21] Manganese Dioxide:International Chemical Safety Cards, International Group of Experts on Behalf of International Labour Organization and World Health Organization, with the Financial Assistance of the European Commission, ILO, WHO, 2021.